

Epitaxial growth and magnetic properties of $\text{Ni}_x\text{Fe}_{4-x}\text{N}$ ($x=0, 1, 3, \text{ and } 4$) films on $\text{SrTiO}_3(001)$ substrates

Fumiya Takata, Keita Ito, Soma Higashikozono, Toshiki Gushi, Kaoru Toko, and Takashi Suemasu

Citation: *Journal of Applied Physics* **120**, 083907 (2016); doi: 10.1063/1.4961734

View online: <http://dx.doi.org/10.1063/1.4961734>

View Table of Contents: <http://scitation.aip.org/content/aip/journal/jap/120/8?ver=pdfcov>

Published by the [AIP Publishing](#)

Articles you may be interested in

[Perpendicular magnetic anisotropy of \$\text{Mn}_4\text{N}\$ films on \$\text{MgO}\(001\)\$ and \$\text{SrTiO}_3\(001\)\$ substrates](#)

J. Appl. Phys. **115**, 17A935 (2014); 10.1063/1.4867955

[Magnetic and structural properties of \$\text{BiFeO}_3\$ thin films grown epitaxially on \$\text{SrTiO}_3/\text{Si}\$ substrates](#)

J. Appl. Phys. **113**, 17D919 (2013); 10.1063/1.4796150

[Structural and magnetic characterizations of \$\text{Mn}_2\text{CrO}_4\$ and \$\text{MnCr}_2\text{O}_4\$ films on \$\text{MgO}\(001\)\$ and \$\text{SrTiO}_3\(001\)\$ substrates by molecular beam epitaxy](#)

J. Appl. Phys. **109**, 07D714 (2011); 10.1063/1.3545802

[Spin and orbital magnetic moments of molecular beam epitaxy \$\gamma'\$ - \$\text{Fe}_4\text{N}\$ films on \$\text{LaAlO}_3\(001\)\$ and \$\text{MgO}\(001\)\$ substrates by x-ray magnetic circular dichroism](#)

Appl. Phys. Lett. **98**, 102507 (2011); 10.1063/1.3564887

[Correlation between structural deformation and magnetoelectric response in \$\(1-x\)\text{Pb}\(\text{Zr}_{0.52}\text{Ti}_{0.48}\)\text{O}_3-x\text{NiFe}_{1.9}\text{Mn}_{0.1}\text{O}_4\$ particulate composites](#)

Appl. Phys. Lett. **91**, 162905 (2007); 10.1063/1.2799261

AIP | Journal of Applied Physics

INTRODUCING INVITED PERSPECTIVES

Ultrafast magnetism and THz spintronics

Authors: Jakob Walowski and Markus Münzenberg

Epitaxial growth and magnetic properties of $\text{Ni}_x\text{Fe}_{4-x}\text{N}$ ($x = 0, 1, 3,$ and 4) films on $\text{SrTiO}_3(001)$ substrates

Fumiya Takata,¹ Keita Ito,^{1,2,3,a)} Soma Higashikozono,¹ Toshiki Gushi,¹ Kaoru Toko,¹ and Takashi Suemasu¹

¹*Institute of Applied Physics, Graduate School of Pure and Applied Sciences, University of Tsukuba, Tsukuba, Ibaraki 305-8573, Japan*

²*Department of Electronic Engineering, Graduate School of Engineering, Tohoku University, Sendai 980-8579, Japan*

³*Japan Society for the Promotion of Science (JSPS), Chiyoda, Tokyo 102-0083, Japan*

(Received 7 June 2016; accepted 16 August 2016; published online 29 August 2016)

The 20–60 nm-thick epitaxial $\text{Ni}_x\text{Fe}_{4-x}\text{N}$ ($x = 0, 1, 3,$ and 4) films were successfully fabricated on $\text{SrTiO}_3(001)$ single-crystal substrates by alternating the substrate temperature (T_{sub}), and their crystalline qualities and magnetic properties were investigated. It was found that the crystal orientation and the degree of order of N site were improved with the increase of T_{sub} for $x = 1$ and 3 . The lattice constant and saturation magnetization decreased as the Ni content increased. This tendency was in good agreement with first-principle calculation. Curie temperature of the Ni_3FeN film was estimated to be 266 K from the temperature dependence of magnetization. The Ni_4N film was not ferromagnetic but paramagnetic due to its low degree of order of N site. *Published by AIP Publishing.*

[<http://dx.doi.org/10.1063/1.4961734>]

I. INTRODUCTION

In recent years, great attention has been paid to anti-perovskite type $3d$ transition metal ferromagnetic nitrides as a new spintronics material due to their excellent electronic and magnetic properties. The crystal structure of these materials is shown in Fig. 1, in which the transition metal atoms occupy the corner (I) and face-center (II) sites and the N atom occupies the body-center site. The II sites can be further classified into IIA and IIB. Fe_4N , one of these compounds, is theoretically predicted to have a very large negative spin-polarization of electrical conductivity.¹ The high spin-polarization of Fe_4N was experimentally demonstrated via the point-contact Andreev reflection technique and the large tunneling magnetoresistance (TMR) effect in the magnetic tunneling junction (MTJ) with Fe_4N electrodes.^{2,3} Moreover, an inverse TMR ratio of -75% in $\text{CoFeB}/\text{MgO}/\text{Fe}_4\text{N}$ MTJs and negative anisotropic magnetoresistance (AMR) effects, originating from the negative spin-polarization of Fe_4N , were reported.⁴⁻⁸

Substitution of other $3d$ transition metal atoms for Fe in the Fe_4N lattice is an effective means to modify their magnetic properties. For example, $\text{Co}_x\text{Fe}_{4-x}\text{N}$, where Fe atoms are partially replaced with Co atoms, is theoretically expected to exhibit a larger negative spin-polarization of density of states (DOS) at Fermi level (E_F) than Fe_4N .⁹ Up to now, we have succeeded in fabricating these binary $3d$ nitrides such as $\text{Co}_x\text{Fe}_{4-x}\text{N}$ and $\text{Co}_x\text{Mn}_{4-x}\text{N}$ by molecular beam epitaxy (MBE) and revealed their magnetic and transport properties.¹⁰⁻¹⁶

In this work, we focused on $\text{Ni}_x\text{Fe}_{4-x}\text{N}$. There have been several reports both by theory and by experiment on $\text{Ni}_x\text{Fe}_{4-x}\text{N}$, especially for $x \leq 2.4$.¹⁷⁻²⁷ NiFe_3N has some

similarities with Ni-Fe Invar alloys from the viewpoints of thermal expansion and forced magnetostriction¹⁷ and has a magnetic moment of $7.15 \mu_B$ per formula unit.¹⁸ The structural and magnetic properties of $\text{Ni}_x\text{Fe}_{4-x}\text{N}$ (up to $x = 2.4$) films grown on Si or glass substrates were reported.²³⁻²⁷ In contrast, studies on $\text{Ni}_x\text{Fe}_{4-x}\text{N}$ with higher Ni compositions ($x > 2.4$) have been quite limited. Diao *et al.* demonstrated that the lattice constant, the saturation magnetization (M_s), and Curie temperature (T_c) of powdered $\text{Ni}_x\text{Fe}_{4-x}\text{N}$ ($0 \leq x \leq 3.6$) monotonically decreased with increasing x . According to their results, T_c is 287 K, slightly lower than the room temperature (RT) for $x \geq 3$.²⁸ However, this is inconsistent with a recent report showing that the T_c of Ni_3FeN is above RT because Ni_3FeN epitaxial films exhibited a large positive AMR ratio of approximately 6% at RT.²⁹ For these reasons, the T_c of Ni_3FeN has not been determined yet. In addition, we have only limited information about the magnetic properties of Ni_4N .³⁰⁻³³ In this article, we fabricated 20–60 nm-thick $\text{Ni}_x\text{Fe}_{4-x}\text{N}$ epitaxial films in a wide range of $0 \leq x \leq 4$ and examined their

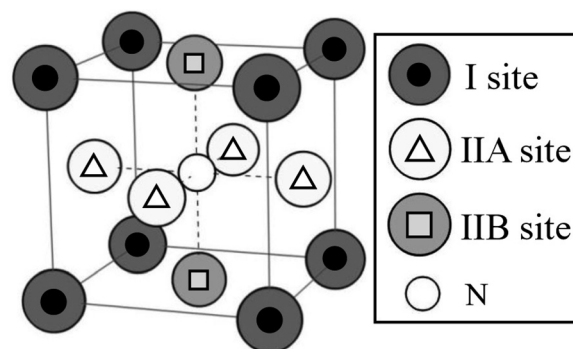


FIG. 1. Crystal structure of anti-perovskite type $3d$ transition metal ferromagnetic nitrides. II site can be divided into IIA and IIB site.

^{a)}Electronic mail: keita.ito.729@gmail.com

TABLE I. Calculated formation energy (E_{form}), lattice parameters (a , c), magnetic moment (m_{spin}), saturation magnetization (M_s), and spin-polarization (P_D) of $\text{Ni}_x\text{Fe}_{4-x}\text{N}$ ($x=0, 1, 3$, and 4).

Compounds	E_{form} (eV/f.u.)	a (nm)	c (nm)	m_{spin} (μ_B /f.u.)	M_s (emu/cm ³)	P_D
Fe_4N	-0.2454	0.37902	0.37902	9.977	1669	-0.49
NiFe_3N (A-type)	-0.332	0.37726	0.37726	8.008	1383	-0.55
NiFe_3N (B-type)	-0.2927	0.37988	0.37178	8.073	1395	-0.39
Ni_3FeN (A-type)	0.5273	0.37604	0.37604	4.105	716	-0.86
Ni_3FeN (B-type)	-0.0213	0.37302	0.3784	4.067	716	-0.53
Ni_4N	0.449	0.37224	0.37224	1.494	269	-0.38

fundamental properties in detail comparing with first-principle calculation.

II. METHOD

A. Experiments

We grew 20–60 nm-thick $\text{Ni}_x\text{Fe}_{4-x}\text{N}$ ($x=0, 1, 3$, and 4) films on SrTiO_3 (STO) (001) single-crystal substrates by MBE using solid sources of Ni and/or Fe and radio-frequency (RF) N plasma. Substrate temperature (T_{sub}) was varied from 150 to 550 °C and the RF power was set to 105 W. The Ni/Fe ratio was controlled by their crucible temperatures. The crystalline quality of grown films was evaluated by reflection high-energy electron diffraction (RHEED) observed along the STO[100] axis, out-of-plane ($\omega-2\theta$) x-ray diffraction (XRD), and in-plane ($\phi-2\theta\chi$) XRD measurements with Cu-K α

radiation. As a measure of the occupation probability of N atom at the body center of $\text{Ni}_x\text{Fe}_{4-x}\text{N}$, the degree of order (S), defined by Eqs. (1) and (2),^{8,34} is utilized.

$$S = \sqrt{\frac{I_{100}^{\text{obs}}/I_{200}^{\text{obs}}}{I_{100}^{\text{cal}}/I_{200}^{\text{cal}}}}, \quad (1)$$

$$I_{hkl}^{\text{cal}} = LP \cdot \psi \cdot F_{hkl}^2 \cdot \exp\left(-2B \frac{\sin^2\theta}{\lambda^2}\right), \quad (2)$$

where I_{hkl}^{obs} and I_{hkl}^{cal} are the integrated XRD intensities of the (hkl) plane obtained by experiment and calculation, respectively. In Eq. (2), LP is the Lorentz-polarization factor for single-crystal, ψ is the powder ring distribution factor,³⁵ the exponential term is the Debye-Waller factor, and F_{hkl} is the structure factor of $\text{Ni}_x\text{Fe}_{4-x}\text{N}$ unit cell for (hkl) diffraction. For the in-plane XRD geometry, ψ is obtained by Eq. (5) in Ref. 35, the equipment parameter s_2 was fixed to be 3.3° by replacing with the angular divergence of the detector window. F_{hkl} was calculated using Eq. (3) by assuming that Ni and Fe atoms are randomly distributed over I and II sites. F_{hkl} is given by

$$F_{hkl} = \left(\frac{x \cdot f_{\text{Ni}} + (4-x) \cdot f_{\text{Fe}}}{4}\right) \{1 + (-1)^{h+k} + (-1)^{k+l} + (-1)^{l+h}\} + f_{\text{N}}(-1)^{h+k+l}. \quad (3)$$

For the calculation of F_{hkl} , we adapted the electron structure of $\text{Fe}^0(\text{Fe}^{+1/3})_3\text{N}^{-1}$ for Fe_4N ³⁶ and assumed that the electron number of Ni, Fe, and N atoms for NiFe_3N and Ni_3FeN were Ni^0 , Fe^0 , and N^0 , respectively. The atomic scattering factors f_{Ni} , f_{Fe} , and f_{N} for Ni^0 , Fe^0 , and N^0 were given in Refs. 37

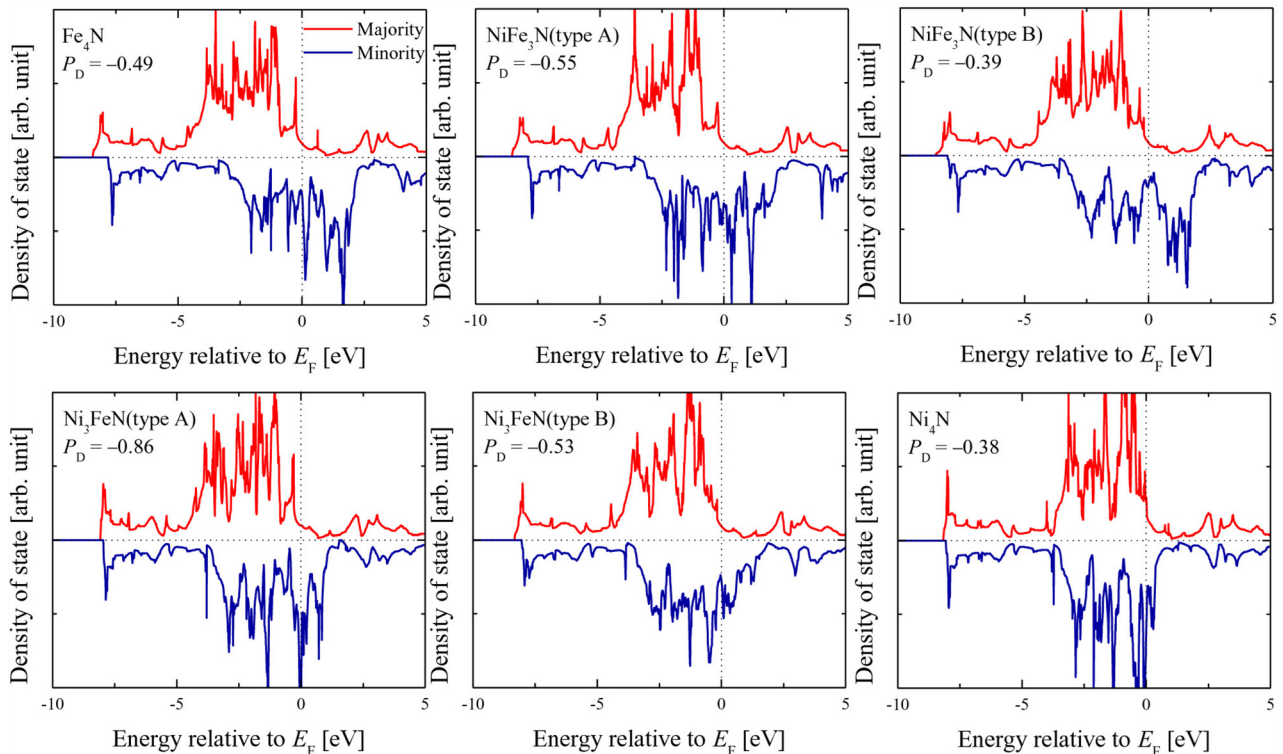


FIG. 2. Calculated spin-polarized density of states of $\text{Ni}_x\text{Fe}_{4-x}\text{N}$ ($x=0, 1, 3$, and 4).

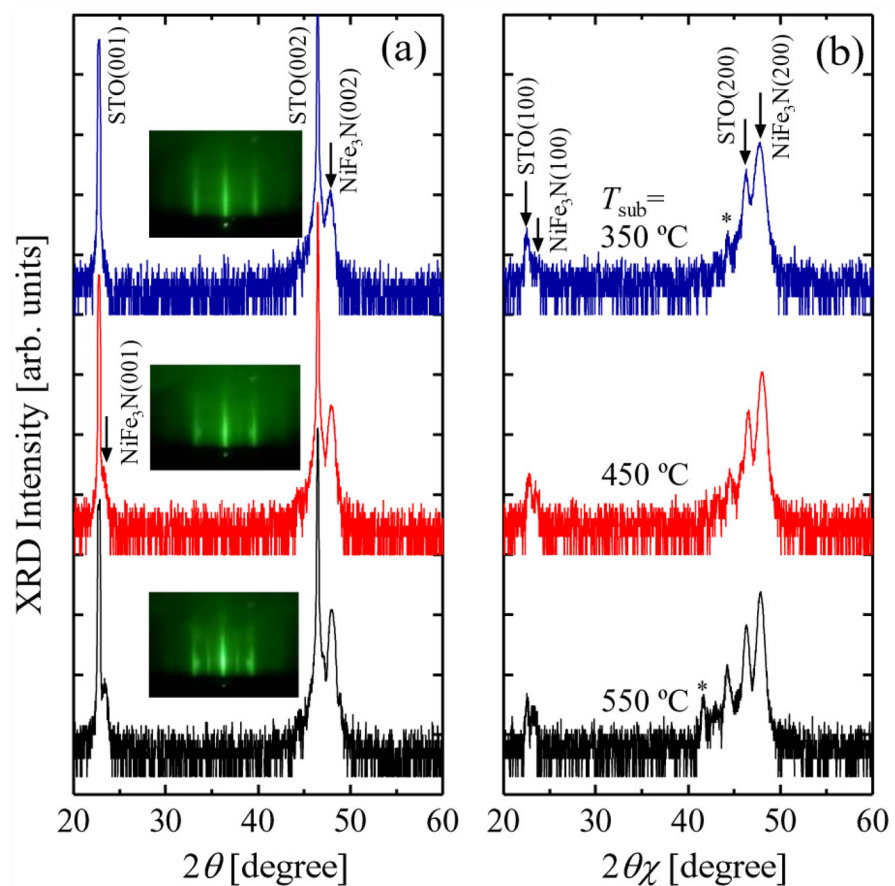


FIG. 3. RHEED, (a) ω - 2θ XRD, and (b) ϕ - $2\theta\chi$ XRD patterns of NiFe₃N films. The peaks labeled with an asterisk indicate the diffractions caused by the Cu-K β or W-L α x-rays.

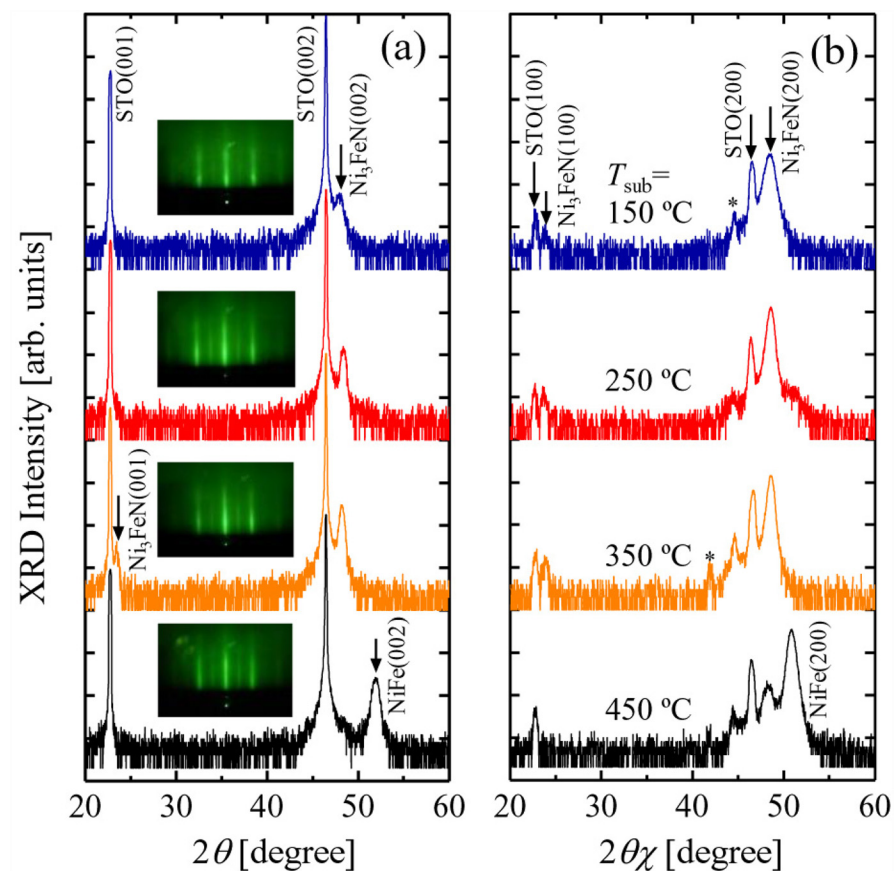


FIG. 4. RHEED, (a) ω - 2θ XRD, and (b) ϕ - $2\theta\chi$ XRD patterns of Ni₃FeN films.

and 38, and that for $\text{Fe}^{+1/3}$ was obtained by the interpolation of the Fe^0 and Fe^{+1} data. The standard deviation of tilt angles of Fe_4N , NiFe_3N , and Ni_3FeN were, respectively, determined as 0.54° , 0.45° , and 0.71° from the $\ln(I_{hkl}^{obs})$ versus $(\Delta\omega)^2$ plots for $\text{Ni}_x\text{Fe}_{4-x}\text{N}$ (002) diffraction.³⁵ The offset angle $\Delta\omega$ from the usual ω angle in the ω - 2θ XRD measurement was varied as $\pm 0.1^\circ$, 0.25° , 0.5° , 0.75° , 1.0° , or 1.5° . The temperature parameter B was calculated by plotting $\ln\{I_{hkl}^{obs}/(LP \cdot \psi \cdot F_{hkl}^2)\}$ against $\sin^2\theta/\lambda^2$ using the fundamental diffraction peaks of (200), (220), and (400).^{36,39} Magnetic measurements were carried out for approximately 60 nm-thick $\text{Ni}_x\text{Fe}_{4-x}\text{N}$ films utilizing the vibrating sample magnetometer (VSM) and superconducting quantum interference device (SQUID) magnetometer. The $\text{Ni}_x\text{Fe}_{4-x}\text{N}$ layer thicknesses with surface oxides subtracted were determined by x-ray reflectometry analysis.

B. Calculation details

We performed first-principle calculation for $\text{Ni}_x\text{Fe}_{4-x}\text{N}$ ($x=0, 1, 3,$ and 4) using Vienna *ab initio* simulation package⁴⁰ (VASP) with the projected-augment wave pseudopotential,⁴¹ spin-polarized Perdew-Burke-Ernzerhof generalized gradient approximations,⁴² and Bader charge analysis.⁴³ The total energy minimization was obtained via an optimization of the lattice parameters and a relaxation of the atomic positions in a conjugate gradient routine. The convergence in the total energy was better than 10^{-7} eV/f.u. using the energy cut off of 400 eV. The k -points sampling of $11 \times 11 \times 11$ were used for the calculation of the charge density with VASP. Performing the calculation of structural relaxation, formation energy (E_{form}), lattice parameters (a and c), spin magnetic moment (m_{spin}), saturation magnetization (M_s), density of states (DOS) of majority and minority spins (D_\uparrow and D_\downarrow), and spin-polarized DOS at E_F [$P_D = (D_\uparrow - D_\downarrow) / (D_\uparrow + D_\downarrow)$] were calculated. The total electronic energies for fcc-Ni, bcc-Fe, and molecular N_2 were also calculated to estimate E_{form} .⁴⁴ We considered two types of model for NiFe_3N and Ni_3FeN . In a unit cell of NiFe_3N (Ni_3FeN), Ni (Fe) atoms are located at I site and Fe (Ni) atoms are at II site in A-type, while Fe (Ni) atoms are located at I and IIA sites, and Ni (Fe) atoms are at IIB site in B-type.

III. RESULTS AND DISCUSSION

Table I shows the E_{form} , a , c , m_{spin} , M_s , and P_D of $\text{Ni}_x\text{Fe}_{4-x}\text{N}$ ($x=0, 1, 3,$ and 4) and Fig. 2 illustrates their D_\uparrow and D_\downarrow obtained from first-principle calculation. Calculations show that all compositions examined are ferromagnetic. It should be noted that the highest value of $P_D = -0.86$ was obtained for A-type Ni_3FeN . This result suggests that A-type Ni_3FeN can be a candidate material for spintronics with a high spin-polarization. Focusing on the sign and magnitude of E_{form} , we can discuss whether these compounds are stable or not. E_{form} was, however, 0.5273 eV/f.u. for A-type Ni_3FeN , which is positive and much higher than $E_{\text{form}} = -0.0213$ eV/f.u. for B-type Ni_3FeN with smaller $P_D = -0.53$, implying that A-type is not stable. This calculation supports the experimental report that Ni atoms preferentially replaced Fe atoms located at I site in Fe_4N .^{21,22} Although E_{form} is negative for B-

type Ni_3FeN , it is much larger than that for Fe_4N or NiFe_3N . Furthermore, Ni_4N and A-type Ni_3FeN have positive E_{form} , suggesting that Ni_3FeN and Ni_4N are unstable. The interesting point is that tetragonal modification occurs for B-type NiFe_3N and Ni_3FeN with c/a ratios of 0.98 and 1.01, respectively.

Figures 3 and 4 show ω - 2θ XRD, ϕ - $2\theta\chi$ XRD, and RHEED patterns of 20 nm-thick NiFe_3N and Ni_3FeN films, respectively. T_{sub} was changed from 350 to 550 °C for NiFe_3N and 150 to 450 °C for Ni_3FeN . Streaky RHEED patterns and only (001) oriented diffraction peaks were observed for all the grown films deposited at 150–350 °C, which is indicative of epitaxial growth of single-phase nitrides. When T_{sub} was above 400 °C for Ni_3FeN , the diffraction peak of $\text{NiFe}(002)$ was observed, suggesting the decomposition of Ni_3FeN to NiFe due to the release of N atoms. The T_{sub} dependences of the full width at half maximum (FWHM) for $\text{NiFe}_3\text{N}(002)$ and $\text{Ni}_3\text{FeN}(002)$ diffraction lines, measured by x-ray ω -scan rocking curves and S , are plotted in Fig. 5. With increasing T_{sub} , the FWHMs for $\text{NiFe}_3\text{N}(002)$ and $\text{Ni}_3\text{FeN}(002)$ diffraction lines decreased and showed the smallest values of 0.280 and 1.248° at $T_{\text{sub}} = 550$ and 400°C , respectively; their S reached the largest values of 0.71 and 0.75 , respectively. The decreasing of FWHM indicates the enlargement of grain size or the reduction of inhomogeneous strain in the films, and the

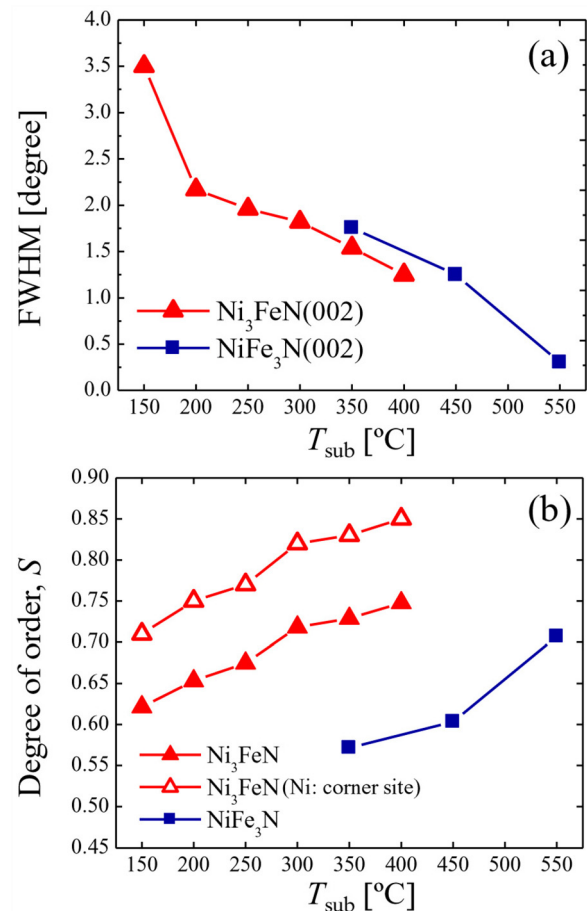


FIG. 5. Temperature dependence of (a) FWHM for $\text{NiFe}_3\text{N}(002)$ and $\text{Ni}_3\text{FeN}(002)$ diffraction line and (b) degree of order (S) of N site. The red outlined triangles in Fig. 5(b) are the S values assuming Ni atom perfectly occupies I sites in the lattice.

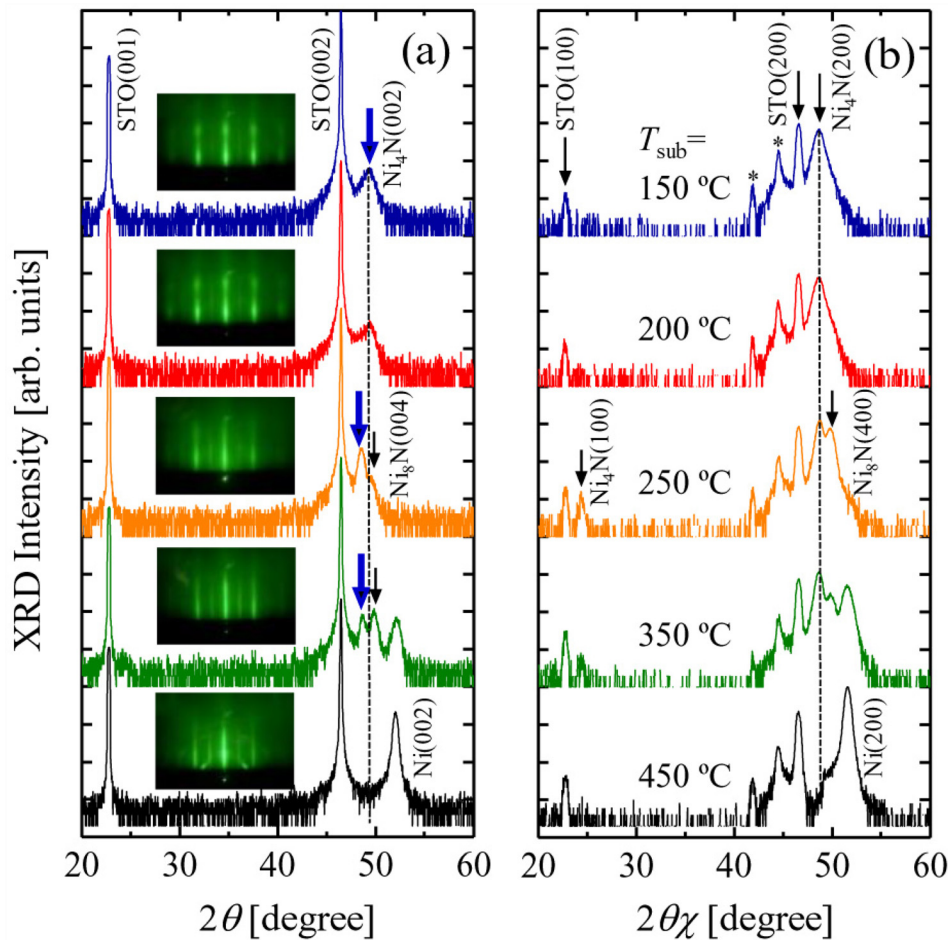


FIG. 6. RHEED, (a) ω - 2θ XRD, and (b) ϕ - $2\theta\chi$ XRD patterns of Ni_4N films. The broken lines are a guide to the eye.

enhancement of S values was caused by the promotion of N diffusion by heating during deposition. According to Mössbauer spectroscopy study on $\text{Ni}_x\text{Fe}_{4-x}\text{N}$, the Ni atoms completely occupy I sites at $x \geq 2$.²² We therefore assumed that I sites were occupied by Ni atoms in Ni_3FeN and calculated the S values to be 0.71, 0.75, 0.77, 0.82, 0.83, and 0.85 for films grown at $T_{\text{sub}} = 150, 200, 250, 300, 350,$ and 400 °C, respectively, as shown in Fig. 5(b), by using Eqs. (1) and (2). The S values were larger by about 0.1 than those for Ni atoms randomly occupying I and II sites at all T_{sub} due to the modulation of F_{hkl} .

Figure 6 shows ω - 2θ XRD, ϕ - $2\theta\chi$ XRD, and RHEED patterns of 20 nm-thick Ni_4N films deposited at various T_{sub} ranging from 150 to 450 °C. Only (001) oriented diffraction peaks and streaky RHEED patterns were obtained for films grown at 150 and 200 °C, showing that single-phase Ni_4N was epitaxially grown. However, other phases such as Ni_8N and Ni were confirmed at $T_{\text{sub}} = 250, 350,$ and 450 °C. Ni_8N is an intermediate phase formed during the decomposition of Ni_4N to fcc-Ni.³³ In the ω - 2θ XRD profiles of samples grown at $T_{\text{sub}} = 150$ and 200 °C, the diffraction peak of $\text{Ni}_4\text{N}(002)$ shifted to higher angles, whereas the $\text{Ni}_4\text{N}(200)$ peak did not shift in the ϕ - $2\theta\chi$ XRD profiles, meaning that the in-plane tensile strain exists in the Ni_4N grown at low temperature. An out-of-plane lattice constant (c) to in-plane lattice constant (a) ratio (c/a) was approximately 0.98, determined from the diffraction lines of $\text{Ni}_4\text{N}(002)$ and $\text{Ni}_4\text{N}(200)$ in the ω - 2θ XRD and ϕ - $2\theta\chi$ XRD profiles. The fact that Ni_3FeN and

Ni_4N films were easily decomposed to other phases is supported by our calculation showing that they are not stable because their E_{form} are positive as shown in Table I. The S value was calculated to be 0.76 for Fe_4N fabricated at $T_{\text{sub}} = 450$ °C, whereas we were not able to calculate it for Ni_4N because of its super lattice diffraction peak being very weak. The lattice constants deduced from the XRD patterns and those from first-principle calculation (A-type NiFe_3N and

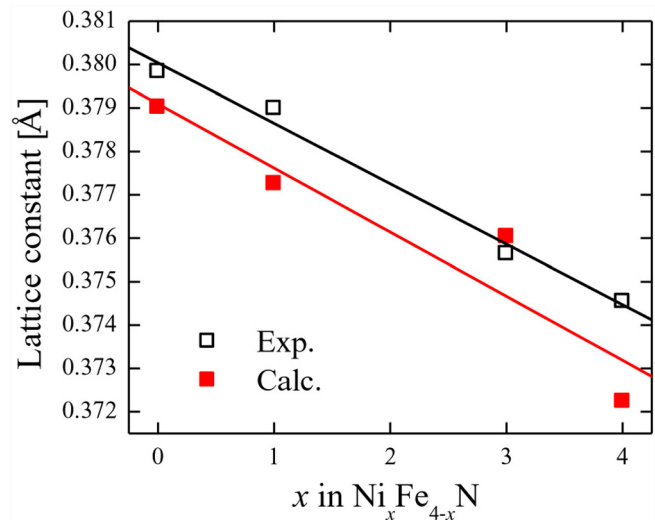


FIG. 7. Lattice constants of $\text{Ni}_x\text{Fe}_{4-x}\text{N}$ ($x = 0, 1, 3,$ and 4) thin films as a function of Ni content.

TABLE II. In-plane lattice constant a , out-of-plane lattice constant c , and cube root of unit cell volume $V = a^2c$ deduced from the XRD patterns of the samples.

Compounds	a (nm)	c (nm)	$\sqrt[3]{V}$ (nm)
Fe ₄ N	0.3798	0.3798	0.3798
NiFe ₃ N	0.3790	0.3788	0.3789
Ni ₃ FeN	0.3749	0.3770	0.3756
Ni ₄ N	0.3739	0.3756	0.3745

Ni₃FeN) are plotted as a function of Ni concentration in Fig. 7. The lattice parameters were determined experimentally by Cohen's method adapting Nelson-Riley function⁴⁵ for Ni_xFe_{4-x}N ($x=0, 1, 3$, and 4) films fabricated at $T_{\text{sub}} = 450, 550, 350$, and 250°C , respectively. They showed the smallest FWHMs at these T_{sub} . Table II summarizes the in-plane lattice constant a , out-of-plane lattice constant c , and cube root of the unit cell volume $V = a^2c$ of the samples deduced from the positions of the Bragg angles of Ni_xFe_{4-x}N(001), (100), (110), (002), (200), (220), (004), and (400) in the XRD patterns. Note that Ni₄N(001) and (110) diffractions were not used because they were not detected. The decrease of lattice constants with increasing x in Ni_xFe_{4-x}N is well explained by the

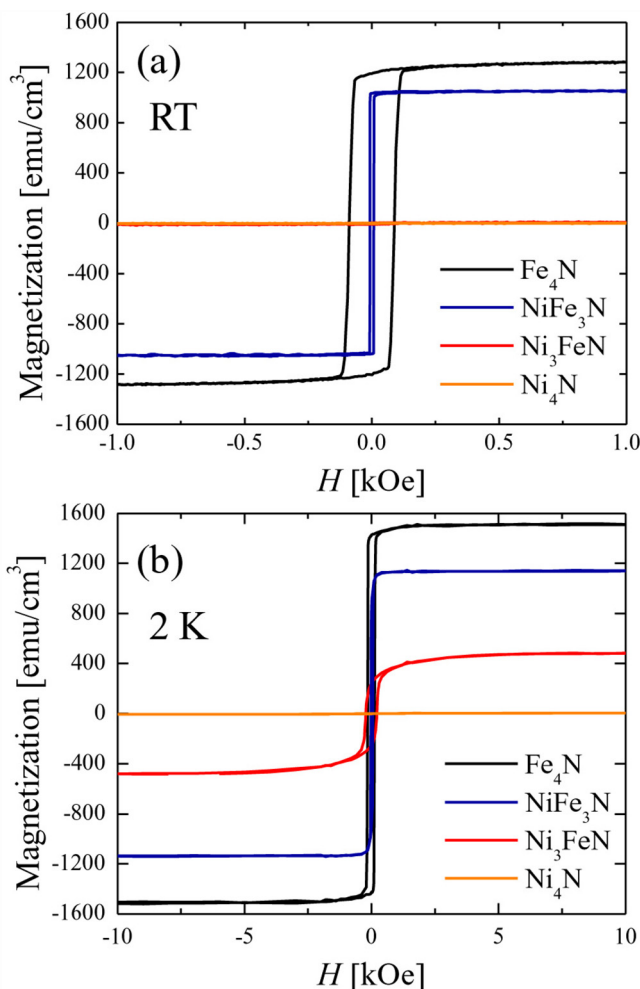


FIG. 8. Magnetization curves of Ni_xFe_{4-x}N ($x=0, 1, 3$, and 4) thin films measured at (a) RT and (b) 2 K when the magnetic field was applied along Ni_xFe_{4-x}N[100] direction.

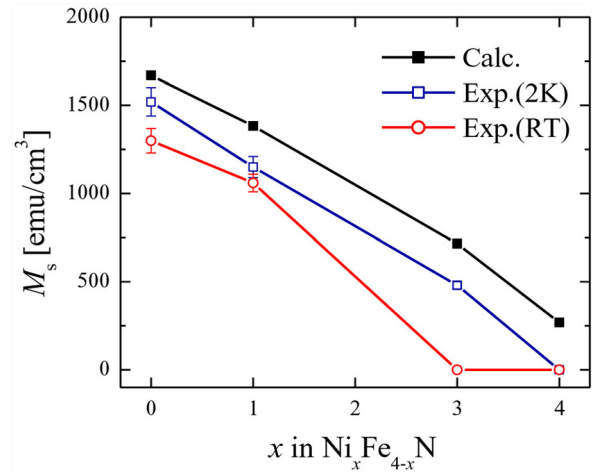


FIG. 9. Saturation magnetization of Ni_xFe_{4-x}N ($x=0, 1, 3$, and 4) thin films as a function of Ni concentration.

replacement of Fe atoms with smaller radius Ni atoms. The epitaxial relationship between STO and Ni_xFe_{4-x}N was found to be STO[100](001) || Ni_xFe_{4-x}N[100](001). In this relation, the lattice mismatches are about -3% to -4% and epitaxial growth was successfully achieved owing to these small lattice mismatches.

Figures 8(a) and 8(b), respectively, show the magnetization curve measured at RT and 2 K using VSM or SQUID. The samples used for the measurement were approximately 60 nm-thick Ni_xFe_{4-x}N ($x=0, 1, 3$, and 4) films grown at $T_{\text{sub}} = 450, 550, 350$, and 150°C , respectively. External magnetic field H was applied to the Ni_xFe_{4-x}N[100] axis. Figure 9 shows the M_s of Ni_xFe_{4-x}N films as a function of x . Those obtained from first-principle calculation are also plotted. The M_s values were $1300 \pm 70 \text{ emu/cm}^3$ and $1060 \pm 50 \text{ emu/cm}^3$ for Fe₄N and NiFe₃N, respectively, at RT, and they increased to $1520 \pm 80 \text{ emu/cm}^3$ and $1150 \pm 60 \text{ emu/cm}^3$ at 2 K. In contrast, the hysteresis curve was not obtained for Ni₃FeN at RT but at 2 K with $M_s = 480 \pm 20 \text{ emu/cm}^3$. The decrease of M_s with increasing Ni content can be mainly attributed to the

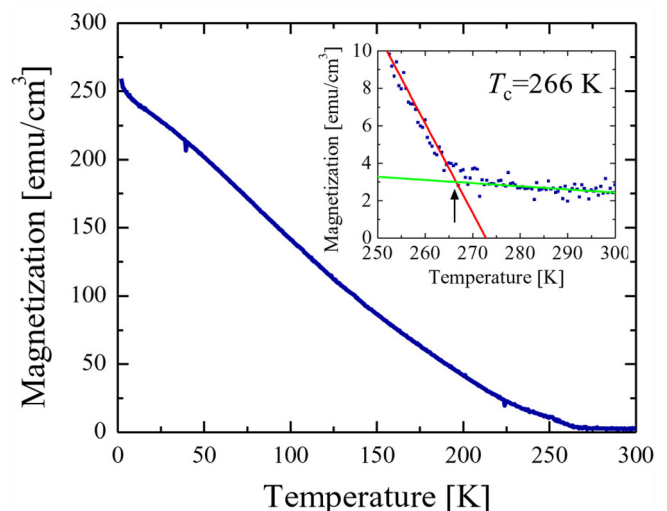


FIG. 10. Temperature dependence of magnetization of Ni₃FeN film when the applied magnetic field was 10 Oe.

substitution of Fe atom by Ni atom with a much smaller spin magnetic moment than Fe atom. Figure 10 shows the temperature dependence of magnetization of Ni₃FeN measured at $H = 10$ Oe applied along the Ni₃FeN[100] axis, and T_c was determined to be 266 K. This value is close to 287 K evaluated by Diao *et al.*²⁸ In our present experimental result, Ni₄N was paramagnetic, differently from our first-principle calculation and others^{46,47} based on the assumption that the perfect degree of order of N atoms in a Ni₄N lattice. The magnetization of our Ni₄N film was much smaller than that of other compositions as shown in Fig. 8(b); which was smaller than 10 emu/cm³ even at 2 K, probably arising from a small amount of residual fcc-Ni in the grown films. According to Ref. 47, they insisted that Ni₄N become a paramagnetic phase when N atoms are located at positions next to each Ni atom.⁴⁷ As mentioned above, the super lattice diffraction attributed to the long range order of N atoms is very weak in the Ni₄N film of this work, meaning that a large number of Ni atoms are located side by side with N atoms. We therefore consider that the Ni₄N film is paramagnetic rather than ferromagnetic due to its low degree of order of N site in the present work.

IV. CONCLUSION

Ni_xFe_{4-x}N ($x = 0, 1, 3,$ and 4) epitaxial films were successfully prepared on STO(001) single-crystal substrates and their magnetic properties were investigated. The crystalline quality and S values were evaluated for samples grown at various T_{sub} . With increasing T_{sub} , the FWHMs of NiFe₃N(002) and Ni₃FeN(002) diffraction lines decreased and they reached the smallest values of 0.28° and 1.248° at $T_{\text{sub}} = 550$ and 400 °C, respectively, and their S values reached the highest values of 0.71 and 0.75. The lattice parameters and M_s decreased for Ni_xFe_{4-x}N as the Ni composition increased. These results were in good agreement with our first-principle calculation except that Ni₄N did not show ferromagnetism even at 2 K. T_c was estimated to be 266 K for Ni₃FeN from the temperature dependence of magnetization.

ACKNOWLEDGMENTS

This work was financially supported in part by JSPS Grants-in-Aid for Scientific Research (A) (No. 26249037) and JSPS Fellows (No. 14J01804). Magnetization measurements were performed with the help of Mr. R. Ishikawa and Professors H. Yanagihara, S. Kuroda, and E. Kita of the University of Tsukuba, and Professor T. Koyano of Cryogenics Division of the University of Tsukuba.

¹S. Kokado, N. Fujima, K. Harigaya, H. Shimizu, and A. Sakuma, *Phys. Rev. B* **73**, 172410 (2006).

²A. Narahara, K. Ito, T. Suemasu, Y. K. Takahashi, A. Ranajikanth, and K. Hono, *Appl. Phys. Lett.* **94**, 202502 (2009).

³K. Sunaga, M. Tsunoda, K. Komasaki, Y. Uehara, and M. Takahashi, *J. Appl. Phys.* **102**, 013917 (2007).

⁴Y. Komasaki, M. Tsunoda, S. Isogami, and M. Takahashi, *J. Appl. Phys.* **105**, 07C928 (2009).

- ⁵M. Tsunoda, Y. Komasaki, S. Kokado, S. Isogami, C. C. Chen, and M. Takahashi, *Appl. Phys. Express* **2**, 083001 (2009).
- ⁶M. Tsunoda, H. Takahashi, S. Kokado, Y. Komasaki, A. Sakuma, and M. Takahashi, *Appl. Phys. Express* **3**, 113003 (2010).
- ⁷K. Ito, K. Kabara, H. Takahashi, T. Sanai, K. Toko, T. Suemasu, and M. Tsunoda, *Jpn. J. Appl. Phys., Part 1* **51**, 068001 (2012).
- ⁸K. Kabara, M. Tsunoda, and S. Kokado, *Appl. Phys. Express* **7**, 063003 (2014).
- ⁹Y. Takahashi, Y. Imai, and T. Kumagai, *J. Magn. Magn. Mater.* **323**, 2941 (2011).
- ¹⁰K. Ito, T. Sanai, S. Zhu, Y. Yasutomi, K. Toko, S. Honda, S. Ueda, Y. Takeda, Y. Saitoh, Y. Imai, A. Kimura, and T. Suemasu, *Appl. Phys. Lett.* **103**, 232403 (2013).
- ¹¹T. Sanai, K. Ito, K. Toko, and T. Suemasu, *J. Cryst. Growth* **378**, 342 (2013).
- ¹²K. Ito, T. Sanai, Y. Yasutomi, S. Zhu, K. Toko, Y. Takeda, Y. Saitoh, A. Kimura, and T. Suemasu, *J. Appl. Phys.* **115**, 17C712 (2014).
- ¹³K. Ito, K. Kabara, T. Sanai, K. Toko, Y. Imai, M. Tsunoda, and T. Suemasu, *J. Appl. Phys.* **116**, 053912 (2014).
- ¹⁴Y. Yasutomi, K. Ito, T. Sanai, K. Toko, and T. Suemasu, *J. Appl. Phys.* **115**, 17A935 (2014).
- ¹⁵K. Ito, T. Sanai, Y. Yasutomi, T. Gushi, K. Toko, H. Yanagihara, M. Tsunoda, E. Kita, and T. Suemasu, *J. Appl. Phys.* **117**, 17B717 (2015).
- ¹⁶K. Ito, Y. Yasutomi, K. Kabara, T. Gushi, S. Higashikozono, K. Toko, M. Tsunoda, and T. Suemasu, *AIP Adv.* **6**, 056201 (2016).
- ¹⁷S. F. Matar, J. G. M. Armitage, P. C. Riedi, G. Demazeau, and P. Hagenmuller, *Eur. J. Solid State Inorg. Chem.* **26**, 517 (1989).
- ¹⁸G. W. Wiener and J. A. Berger, *J. Met.* **7**, 360 (1955).
- ¹⁹Y. Q. Wu and M. F. Yan, *Phys. B* **405**, 2700 (2010).
- ²⁰P. Mohn, K. Schwarz, S. Matar, and G. Demazeau, *Phys. Rev. B* **45**, 4000 (1992).
- ²¹G. Shirane, W. J. Takei, and S. L. Ruby, *Phys. Rev.* **126**, 49 (1962).
- ²²F. Li, J. Yang, D. Xue, and R. Zhou, *Appl. Phys. Lett.* **66**, 2343 (1995).
- ²³S. El Khiraoui, M. Sajieddine, M. Vergnat, M. Sahlaoui, Ph. Bauer, and M. Mabrouki, *J. Alloys Compd.* **440**, 43 (2007).
- ²⁴L. J. Zhu, W. G. Yao, and X. M. Wu, *J. Appl. Phys.* **93**, 4704 (2003).
- ²⁵P. Prieto, J. Camarero, N. Sacristan, D. O. Boerma, and J. M. Sanz, *Phys. Status Solidi A* **203**, 1442 (2006).
- ²⁶P. Prieto, K. R. Pirota, J. M. Sanz, E. Jimenez, J. Camarero, F. Maccherozzi, and F. G. Panaccione, *Appl. Phys. Lett.* **90**, 032505 (2007).
- ²⁷H. Y. Wang, J. Liu, H. S. Huang, W. H. Mao, H. Chen, H. Y. Zhang, Y. J. He, and E. Y. Jiang, *J. Appl. Phys.* **91**, 1453 (2002).
- ²⁸X. G. Diao, A. Y. Takeuchi, F. Garcia, R. B. Scorzelli, and H. R. Rechenberg, *J. Appl. Phys.* **85**, 4485 (1999).
- ²⁹R. Loloee, *J. Appl. Phys.* **112**, 023902 (2012).
- ³⁰N. Terao, *J. Phys. Soc. Jpn.* **15**, 227 (1960).
- ³¹S. Nagakura, N. Otsuka, and Y. Hirotsu, *J. Phys. Soc. Jpn.* **35**, 1492 (1973).
- ³²A. I. Linnik, A. M. Prudnikov, R. V. Shalaev, T. A. Linnik, V. N. Varyukhim, S. A. Kostyrya, and V. V. Burkhovskii, *Tech. Phys. Lett.* **39**, 143 (2013).
- ³³I. M. Neklyudov and A. N. Morozov, *Phys. B* **350**, 325 (2004).
- ³⁴K. Kabara and M. Tsunoda, *J. Appl. Phys.* **117**, 17B512 (2015).
- ³⁵R. C. Reynolds, Jr., *Clays Clay Miner.* **34**, 359 (1986).
- ³⁶S. Nagakura, *J. Phys. Soc. Jpn.* **25**, 488 (1968).
- ³⁷A. J. Freeman, *Acta Crystallogr.* **12**, 261 (1959).
- ³⁸R. E. Watson and A. J. Freeman, *Acta Crystallogr.* **14**, 27 (1961).
- ³⁹N. Elliott, *Phys. Rev.* **129**, 1120 (1963).
- ⁴⁰G. Kresse and J. Furthmüller, *Comput. Mater. Sci.* **6**, 15 (1996).
- ⁴¹P. E. Blöchl, *Phys. Rev. B* **50**, 17953 (1994).
- ⁴²J. P. Perdew, K. Burke, and M. Ernzerhof, *Phys. Rev. Lett.* **77**, 3865 (1996).
- ⁴³G. Henkelman, A. Arnaldsson, and H. Jonsson, *Comput. Mater. Sci.* **36**, 354 (2006).
- ⁴⁴C. M. Fang, M. A. van Huis, J. Jansen, and H. W. Zandbergen, *Phys. Rev. B* **84**, 094102 (2011).
- ⁴⁵S. Okamoto, O. Kitakami, and Y. Shimada, *J. Magn. Magn. Mater.* **208**, 102 (2000).
- ⁴⁶P. Hemzalova, M. Friak, M. Sob, D. Ma, A. Udyansky, D. Raabe, and J. Neugebauer, *Phys. Rev. B* **88**, 174103 (2013).
- ⁴⁷C. M. Fang, R. S. Koster, W. F. Li, and M. A. van Huis, *RSC Adv.* **4**, 7885 (2014).